anticipate that analogs in which the disulfonate pillars have specific functionality will have potential as host lattices for optoelectronic materials, molecular separations, and chemical reactions performed in the nanoscale voids.

## REFERENCES AND NOTES


1. G. M. J. Schmidt, *Pure Appl. Chem.* **27**, 647 (1971); G. R. Desiraju, *Crystal Engineering: The Design of Organic Solids* (Elsevier, New York, 1989).
2. *Comprehensive Supramolecular Chemistry*, J. L. Atwood, J. E. D. Davies, D. D. MacNicol, F. Vogtle, Eds. (Pergamon, New York, 1996), vol. 6; V. Ramamurthy and D. F. Eaton, *Chem. Mater.* **6**, 1128 (1994); J. Wang, M. Simard, J. D. Wuest, *J. Am. Chem. Soc.* **116**, 12119 (1994); G. B. Gardner, D. Venkataraman, J. S. Moore, S. Lee, *Nature* **374**, 792 (1995); B. F. Hoskins and R. Robson, *J. Am. Chem. Soc.* **112**, 1546 (1990); D. M. L. Goodgame, S. Menzer, A. M. Smith, D. J. Williams, *Angew. Chem. Int. Ed. Engl.* **34**, 574 (1995); J. Hulliger, O. Konig, R. Hoss, *Adv. Mater.* **7**, 719 (1995); P. R. Ashton *et al.*, *Angew. Chem. Int. Ed. Engl.* **34**, 1862 (1995); S. V. Kolotuchin, E. E. Fenlon, S. R. Wilson, C. J. Loweth, S. C. Zimmerman, *ibid.*, p. 2654; M. D. Hollingsworth, M. E. Brown, A. C. Hillier, B. D. Santarsiero, J. D. Chaney, *Science* **273**, 1355 (1996); D. Venkataraman, S. Lee, J. Zhang, J. S. Moore, *Nature* **371**, 591 (1994).
3. O. Ermer, *J. Am. Chem. Soc.* **110**, 3747 (1988); _____ and L. Lindenberg, *Helv. Chim. Acta* **74**, 825 (1991).
4. V. A. Russell and M. D. Ward, *Chem. Mater.* **8**, 1654 (1996).
5. G. R. Desiraju, *Angew. Chem. Int. Ed. Eng.* **34**, 2311 (1995).
6. V. A. Russell, M. C. Etter, M. D. Ward, *J. Am. Chem. Soc.* **116**, 1941 (1994); *Chem. Mater.* **6**, 1206 (1994); V. A. Russell and M. D. Ward, *Acta Crystallogr.* **B52**, 209 (1996).
7. Y. P. Zhang and A. Clearfield, *Inorg. Chem.* **31**, 2821 (1992); G. Cao, H.-G. Hong, T. E. Mallouk, *Acc. Chem. Res.* **25**, 420 (1992); M. E. Thompson, *Chem. Mater.* **6**, 1168 (1994); K. P. Reis, V. K. Joshi, M. E. Thompson, *J. Catal.* **161**, 62 (1996); G. Cao and T. E. Mallouk, *J. Solid State Chem.* **94**, 59 (1991).
8. A simple model based on a 2D planar **GS** sheet and idealized cylindrical guests indicates that the diameter of the guest molecule ($D_g$) must be $D_g < 2\sqrt{3} \cdot d_{SS} - D_p$ for the bilayer motif and $D_g < 2 \cdot d_{SS} - D_p$ for the continuous single-layer stacking motif, where $d_{SS}$ is the distance between nearest neighbor sulfur atoms in a **GS** sheet (approximately 7.5 Å), and $D_p$ is the diameter of the pillar as projected onto the **GS** sheet. If the guest is a flat monolith oriented along the channel direction, the width of the guest ($W_g$), as projected onto the **GS** sheet, must be $W_g < \sqrt{3/2} \cdot d_{SS} - D_p$ for the bilayer motif and $W_g < \sqrt{3} \cdot d_{SS} - D_p$ for the continuous single-layer stacking motif.
9. This nonlayered guest-free phase of $(\mathbf{G})_2\mathbf{III}$ also can be crystallized directly from water in the absence of acetonitrile: space group $P2_1/n$, $a$ = 7.958 Å, $b$ = 10.936 Å, $c$ = 8.346 Å, $\beta$ = 92.070°. This phase is identical to that obtained by removal of $CH_3CN$ guests from $(\mathbf{G})_2\mathbf{III} \cdot 2CH_3CN$.
10. Packing fraction values were calculated from Connolly surfaces using Cerius$^2$ molecular modeling software (version 1.6). A comparison of arbitrarily chosen examples from the Cambridge Structural Database revealed that the PF values calculated with Cerius$^2$ are systematically lower, by an average of 1.2%, than Ck values reported by others [see A. I. Kitaigorodskii, *Molecular Crystals and Molecules* (Academic Press, New York, 1973), and A. Gavezzotti, *Nouv. J. Chim.* **6**, 443 (1982)].
11. A nonlayered guest-free phase $(\mathbf{G})_2$(propane-1,3-disulfonate) can be crystallized from water. Molecular models indicate that the voids in a propane-1,3-disulfonate bilayer structure would not be large enough to accommodate molecular guests that would be needed to stabilize the lattice. Furthermore, a bilayer structure would require an unfavorable eclipsed conformation along one of the carbon-carbon bonds of this pillar.
12. The twist angles for biphenyl in the solution and gas phases lie in the ranges 20° to 25° and 40° to 45°, respectively [see O. Bastiansen and S. Samdal, *J. Mol. Struct.* **128**, 115 (1985), and G. Casalone, C. Mariani, A. Mugnoli, M. Simonetta, *Mol. Phys.* **15**, 339 (1968)].
13. The twist angle in crystalline biphenyl is 0°, whereas the twist angles in crystalline substituted biphenyls range from 0° to 47.2° [see G.-P. Charbonneau and Y. Delugeard, *Acta Crystallogr.* **B33**, 1586 (1977), and C. P. Brock and R. P. Minton, *J. Am. Chem. Soc.* **111**, 4586 (1989)].
14. The selectivity profiles for 1-alkanenitriles $CH_3(CH_2)_n$-CN, using $n$ = 5 as a basis, were determined to be 0.13 ($n$ = 6), 1.0 ($n$ = .5), 0.67 ($n$ = 4), 0.04 ($n$ = 3), 0.01 ($n$ = 2), and 0.01 ($n$ = 1). The selectivity trends for 1-alkanols $CH_3(CH_2)_nCH_2OH$, using $n$ = 5 as a basis, were similar, with 1.1 ($n$ = 6), 1.0 ($n$ = 5), 0.71 ($n$ = 4), 0.23 ($n$ = 3), 0.48 ($n$ = 2), and 0.20 ($n$ = 1). The selectivity ratios for 1-alkanenitrile inclusion over 1-alkanol inclusion for equivalent $n$ were 3.0 ($n$ = 6), 6.3 ($n$ = 5), 10.0 ($n$ = 4), and 1.4 ($n$ = 3).
15. M. E. Davis, A. J. Katz, W. R. Ahmad, *Chem. Mater.* **8**, 1820 (1996).


16. We thank V. Young, D. Britton, and W. Ojala (University of Minnesota) for crystallographic services and NSF for financial support. Supplementary material, including crystallographic reports and coordinates, is available on request.

4 December 1996; accepted 7 February 1997


# Scanning Single-Electron Transistor Microscopy: Imaging Individual Charges


M. J. Yoo,* T. A. Fulton, H. F. Hess, R. L. Willett, L. N. Dunkleberger, R. J. Chichester, L. N. Pfeiffer, K. W. West



A single-electron transistor scanning electrometer (SETSE)—a scanned probe microscope capable of mapping static electric fields and charges with 100-nanometer spatial resolution and a charge sensitivity of a small fraction of an electron—has been developed. The active sensing element of the SETSE, a single-electron transistor fabricated at the end of a sharp glass tip, is scanned in close proximity across the sample surface. Images of the surface electric fields of a GaAs/$Al_xGa_{1-x}As$ heterostructure sample show individual photo-ionized charge sites and fluctuations in the dopant and surface-charge distribution on a length scale of 100 nanometers. The SETSE has been used to image and measure depleted regions, local capacitance, band bending, and contact potentials at submicrometer length scales on the surface of this semiconductor sample.


Inspired by the development of the scanning tunneling microscope, a variety of surface scanning probes (*1*) have been developed to measure and map properties of material surfaces on a microscopic scale. In particular, surface electrical properties have been explored with noncontact techniques such as scanning capacitance microscopy (*2*), scanning Kelvin probe microscopy (*3*), and electric-field–sensitive atomic force microscopy (EFM) (*4*). Indeed, the last has in one instance (*5*) shown the remarkable ability to detect the presence of individual charges and to obtain images of insulating surfaces in which a charged spot of one or two electrons is apparent.

We report the development of a low-temperature scanning electrometer operating on a different principle, one which has one to two orders of magnitude greater charge resolution and a similar spatial resolution (100 nm) compared with the EFM. This microscope, the single-electron transistor (SET) scanning electrometer, or SETSE, uses the SET as a probe to sense the electrically induced charge on its small (100 nm) metal island held in proximity to the sample surface (Fig. 1C). It can detect ~1% of an electron charge (0.01$e$). Because all of the important geometrical parameters are known, one can assign a quantitative interpretation to the SETSE signal. Also, during operation the SETSE, unlike the EFM, does not require the application of high electric fields ($10^6$ V $cm^{-1}$) between the tip and surface, an important consideration for many interesting but easily perturbed semiconductor systems. All of these features enable a broader class of experiments to be explored.

As an example, we studied the electric fields at the surface of a semiconductor GaAs/$Al_xGa_{1-x}As$ heterostructure sample. These fields arise from localized charges at and near the surface as well as from the voltage bias and work function of any underlying electrode. Statistical fluctuations in the density of surface charges are evident, although the individual charges are too closely spaced (<10 nm) to be resolved directly. However, we are able to image the more widely spaced individual charges that are produced by brief light exposure. These


Lucent Technologies, Bell Laboratories, Murray Hill, NJ 07974, USA.

*Present address: Philips Laboratories, 345 Scarborough Road, Briarcliff Manor, NY 10510, USA.

photoinduced charges change the surface electric field to reveal isolated, well-resolved sites where dopant atoms or other electron traps have lost or gained an electron. In addition, we acquired images (with <1-mV resolution) of surface potential variations near biased electrodes, images related to band bending near sample edges, and images of surface fields and corresponding local capacitance. We also describe some measurements of the local work function.

The SET is a submicrometer-sized tunneling device whose current flow is governed by the Coulomb blockade effect (6). It consists of a small metal island connected to metal source and drain leads by two small tunnel junctions. The current tunnels through the junctions at a rate determined by the island's electrostatic potential with respect to the source and drain. This potential is in turn controlled by the electric field that the island experiences from external sources, such as fixed charges or capacitively coupled electrodes on a nearby sample (Fig. 1). At low temperature and proper voltage bias, the current flowing through the SET fluctuates periodically as this electric field increases. In fact, the current passes through a full period each time the electric field lines terminating on the island induce a charge of exactly one additional electron (Fig. 1A) (7). Hence, monitoring of the current through the SET as it is scanned over the sample provides a means of mapping the electric field emanating from the sample surface (8).

Fabrication of the SET involves the evaporation of three separate areas of a thin (10 to 20 nm) aluminum film onto a specially shaped glass fiber. The end of the fiber has a shallow conical taper that terminates at the tip in a flat, nearly circular area ~100 nm in diameter (Fig. 1, B and C) (9). A circular patch of film covering the tip constitutes the field-sensitive island. The films for source and drain leads spread out from the edges of the tip and extend up the sides of the fiber to electrical contacts. The source and drain leads are deposited first by separate evaporations from the side and rear. After an in situ exposure to oxygen that creates the oxide tunnel barriers, a final end-on evaporation deposits the island and forms the tunnel junctions. The three electrode shapes are defined by natural shadowing.

The sample described in this work has electrostatic features on a variety of length scales. It is a GaAs/$Al_xGa_{1-x}As$ heterostructure grown by molecular beam epitaxy (Fig. 1C). A δ-doped layer of Si atoms of density $5 \times 10^{12}$ $cm^{-2}$ is grown 22 nm below the sample surface within an $Al_xGa_{1-x}As$ region. Many of these Si atoms ionize and act as electron donors. Most of the electrons are trapped in states at the GaAs surface, whereas a small fraction go to the GaAs/$Al_xGa_{1-x}As$ interface located 60 nm below the sample surface. Here they form a metallic sheet, a two-dimensional electron gas (2DEG) (10). To describe its electrostatic behavior, the sample may be regarded as a conductor (the 2DEG) topped by 60 nm of insulator (with a dielectric constant of 13) containing the donor and surface charge layers (11). Potential fluctuations on short length scales are produced by these charge layers. Electric fields on a larger scale may be produced by the application of a voltage between the 2DEG and a series of 1-μm-wide, 30-nm-thick metal stripes evaporated upon the sample surface. A sufficiently negative voltage applied to one of these gates depletes the 2DEG, driving the electron gas laterally away from its edge.

The SET-tipped fiber is installed in a low-temperature scanning microscope probe stage, allowing three-dimensional positioning of the tip near the sample with subnanometer precision and stability. For best resolution and signal, the tip is held as close to the surface as possible without contact, typically at a height of 25 nm. Electrical contacts (Fig. 1B) enable the application of a voltage $V_b$ between the SET and the 2DEG (or other electrodes) on the sample and also provide the means of biasing the SET and monitoring its current.

The electric field between tip and sample is monitored by recording the SET current $I_{SET}$ as the probe is scanned without feedback in a plane at a fixed height $z$ above the planar sample surface. Collec-

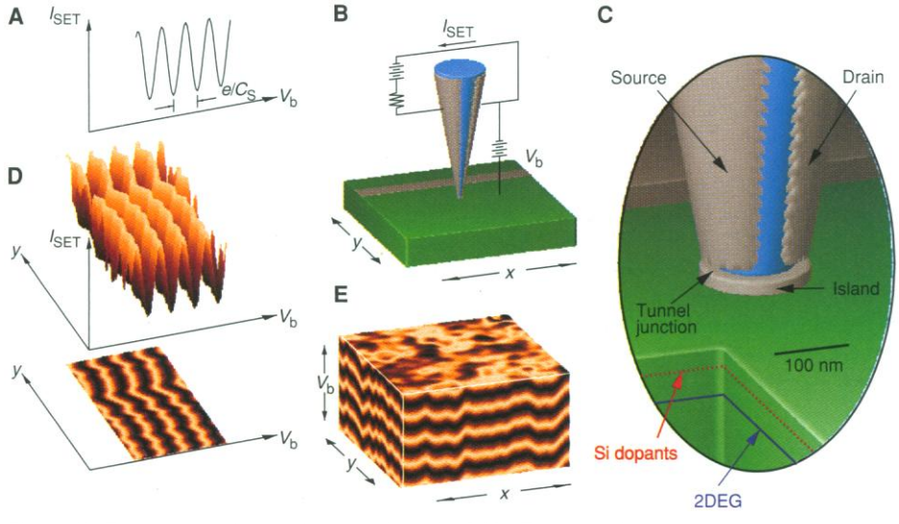


**Fig. 1.** (**A**) Typical current oscillations $I_{SET}(V_b)$ of a SET. (The zero of $I_{SET}$ is offset; the amplitude is actually ~20% of the average). (**B**) Schematic depiction of the SET probe tip suspended above the GaAs/$Al_xGa_{1-x}As$ heterostructure near a gate. (**C**) Magnified view of the tip and a cutaway view of the sample. (**D**) $I_{SET}(V_b)$ versus $y$ for a 2-μm line scan: (top) 3D representations after (A); (bottom) 2D color representation of the same data. The wiggling of the stripes is caused by variations in the electrical charge density of the surface. (**E**) Color representation of a complete data set of $I_{SET}(V_b)$ versus $x$ and $y$ for a 2 μm by 2 μm raster scan over a nongated region. The top of the data block maps the electric field of the sample surface as detected by the SETSE. The side of the block is taken from (D).

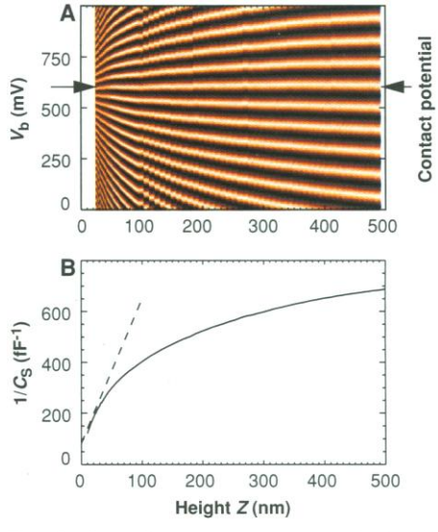


**Fig. 2.** Capacitance versus scan height. (**A**) $I_{SET}(V_b)$ at fixed location ($x$, $y$) along a sequence of heights $z$ above the 2DEG. The convergence of the stripes is caused by proximity to the surface. Arrows indicate the contact potential voltage, from which the local work function can be obtained. (**B**) Inverse capacitance $1/C_s(z)$ as extracted from the period of the data in (A) (solid) and as predicted by parallel plate model (dashed).

tion of a typical data set involves positioning the probe over the surface and sweeping the 2DEG bias voltage $V_b$ by an amount sufficient to cause the induced charge on the island to vary by several electrons. This charge variation in turn causes $I_{SET}(V_b)$ to oscillate through several full cycles, one for each electron (Fig. 1A). A sequence of such curves is taken as the tip is scanned along a line in the $y$ direction (Fig. 1D). Finally, a raster scan in $x$ and $y$ results in a complete $I_{SET}(x, y, V_b)$ data set (Fig. 1E); contour lines in the $xy$ plane indicate lines of constant electric field, with successive contour lines representing electric fields that differ by a fixed amount corresponding to an induced charge of one electron. Acquisition of such a data structure is typical of our measurements.

Because $I_{SET}$ varies nearly sinusoidally with $V_b$ (*12*), we can characterize $I_{SET}$ at each point by a period and a phase. The period ($e/C_s$) (Fig. 1A) is determined by the capacitance $C_s$ between the tip and the sample electrode and varies primarily with height $z$. The phase, which essentially counts the number of electrons induced on the tip, contains most of the information about the spatial distribution of electric fields. It can be regarded as resulting from an effective surface potential $V_s$. That is, one may model the SET current as

$$I_{SET} = A \sin\frac{2\pi Q}{e} = A \sin\frac{2\pi C_s(V_b + V_s)}{e} \quad (1)$$

Here $Q$ is the total charge induced on the probe tip by the sample, expressed as a part $C_sV_b$ due to the electrode bias and a part $C_sV_s$ that accounts for the charge induced by all other sources. Least squares fits of $I_{SET}(V_b)$ at each tip position yield maps of the effective potential $V_s$ and the local capacitance $C_s$ (*13*).

The surface potential $V_s$ can be understood as the sum of two contributions: the work function difference (contact potential) between the probe and sample (*14*) and the potential from charged centers distributed across and below the surface. For every charge beneath the tip, only a fraction $f$ of the total electric flux terminates on the island (*15*): An individual electron charge produces a contribution $fe$ to $Q$ and $fe/C_s$ to $V_s$. The fraction $f$ increases with both lateral and vertical proximity of the probe to the charge, approaching a maximum of 10% for typical scan height of 25 nm. A single electron charge on the surface can then induce $0.1e$ on the probe island (a change in $V_s$ of ~2.5 mV), about 10 times the noise level.

The capacitance $C_s$ depends on the height of the tip above the surface and is used to measure and set this height. A parallel-plate picture predicts that the capacitance varies as $1/z$ when the scan height is small compared with the tip diameter. At large $z$, a weaker $1/\log(z)$ dependence is expected (*16*). The period of the oscillations in $I_{SET}(V_b)$ (Fig. 2A), given by $e/C_s$, decreases sharply as the tip approaches the sample surface. Because the capacitance is infinite for zero separation between the tip and 2DEG, the location of the sample surface can be determined to within 2 nm, allowing for dielectric corrections, by extrapolation of the curve of inverse capacitance versus scan height (Fig. 2B). Fits to the $z$ dependence also give estimates for the tip diameter of order 100 nm.

The local contact potential of the sample can also be extracted from the data of Fig. 2A. An examination shows that there is a bias voltage for which the induced island charge does not vary as the tip is lowered to the sample surface. At this voltage (here ~0.6V), the work function difference between the SET and sample has been nulled. For most SETSE measurements, we operate with a bias approximately nulling the contact potential, which minimizes any perturbation of the sample by electric fields from the tip.

Maps of $V_s$ constructed from $xy$ scans of the same 2DEG region initially show increasingly fine random structure with de-

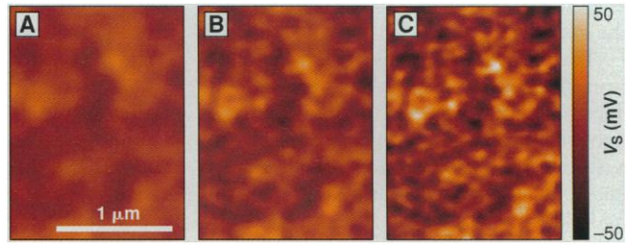


**Fig. 3.** Surface potential $V_s$ in the $xy$ plane (relative to the average value of each image) showing fluctuations from dopants and surface charges as seen at scan heights of (**A**) 95 nm, (**B**) 50 nm, and (**C**) 25 nm. The spatial resolution and sensitivity improve with reduced height.

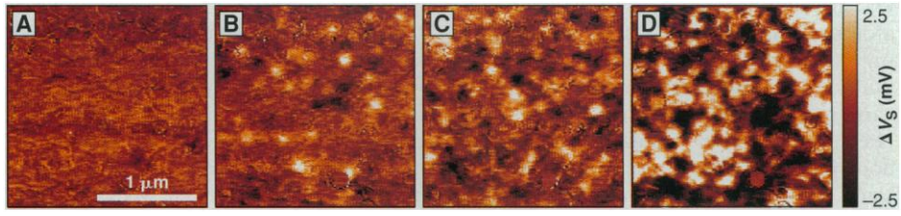


**Fig. 4.** Photoactivity of single dopant atoms and surface traps shown in $xy$ maps of changes in $V_s$ ($\Delta V_s$), induced by exposure to (**A**) no light and light at (**B**) 850 nm, (**C**) 770 nm, and (**D**) 690 nm. Individual photo-ionized (neutralized) sites with a single electron charge are seen as light (dark) spots; that is, light spots mark new positive charges, and dark spots, new negative charges. The sensitivity of the color scale is about an order of magnitude greater than that in Fig. 3.

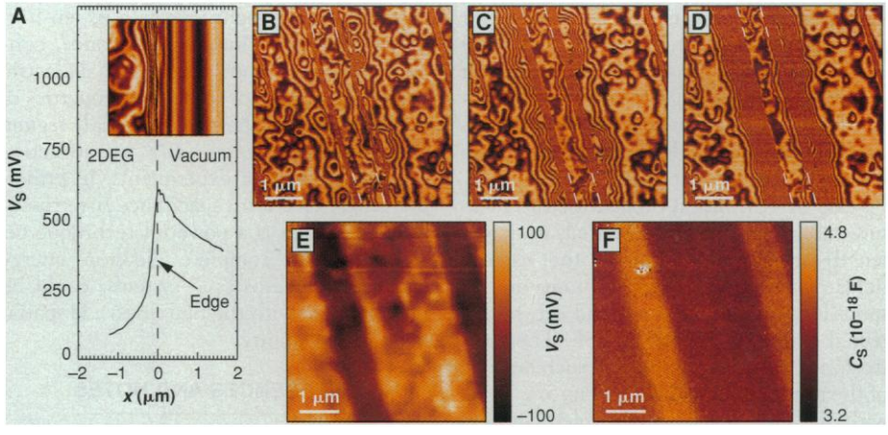


**Fig. 5.** (**A**) Effective surface potential $V_s$ (*21*) measured along a line extending over the cleaved edge of the sample. (Inset) An $xy$ map of $I_{SET}(V_b)$ showing this edge region. (**B** through **D**) $I_{SET}$ $xy$ maps at fixed $V_b$ showing electric field contours produced along a metal gate stripe (outlined by dashed lines) biased at 0, −367, and −733 mV, respectively. (**E**) Surface potential and (**F**) capacitance $xy$ maps derived from a single set of $I_{SET}(V_b, x, y)$ data, showing two metal gate stripes and the intermediate 2DEG region.

creasing $z$ (Fig. 3), eventually revealing 100-nm features. This resolution is limited by the tip diameter. The fluctuation amplitude also increases as the tip approaches the surface, reflecting the enhanced coupling between the SET and sample charges. Typically there are about 300 surface and ionized dopant charges underneath the tip. We believe that the statistical fluctuations in this number across the sample are imaged in Fig. 3C; however, numerical simulations indicate that a random placing of these dopants and trapped charges would produce fluctuations in $V_s$ nearly twice as large as those observed in Fig. 3C, which suggests a more uniform distribution. Such fluctuations in the potential play an important role in limiting the mobility of the underlying 2DEG and give a means of characterizing the disorder.

The SETSE can image individual electron charges on and within the semiconductor sample (Fig. 4). In the absence of light, maps of $V_s$ (Fig. 3) are repeatable to within 1%. This precision allows one to image isolated photo-ionized or neutralized sites (Fig. 4) by subtracting maps made before and after brief, low-intensity illumination. The differences show up as a few small circular spots, presumably donor atoms or traps, whose apparent size (~100 nm) is limited by the spatial resolution. Sufficiently energetic photons create free carriers that can transfer electrons between various sites, primarily the silicon dopants and the surface traps, converting some neutral sites into charged ones and vice versa. The more intense signals are likely from higher (surface) sites, and the weaker signals, from lower (donor layer) sites. Simulations of the charge-coupling fraction $f$ for a single charge of $\pm e$ buried at these levels predict changes in $V_s$ of about 1.5 to 2.5 mV, as observed. The sample is markedly more photoactive for wavelengths above the band gap (760 nm) of the $Al_{0.15}Ga_{0.85}As$ layer. Here greater absorption and a larger number of photogenerated carriers within the $Al_xGa_{1-x}As$ in the region of the donors are responsible for the increased response.

The SETSE has also been used to measure other electrostatic potentials on larger length scales. For example, the electric fields of the charged surface states are responsible for band bending and can be detected externally by the SETSE. The electrostatic potential produced at such an edge of the test sample is shown in Fig. 5A, along with an $I_{SET}$ image of the electric field contour lines (as in Fig. 1E) taken across the same region. The SETSE can also map electrostatic potentials induced by applied gate voltages (Fig. 5, B through D). With successively higher gate voltages (Fig. 5, C and D), more electric field contour lines appear bordering the gate, spreading to nearly 1 μm away, well beyond the expected (*17*) depletion length of 80 nm. Surface potential changes at such distances from the gate are sometimes observed to be hysteretic and may result from charge injection into the surface or dopant layers.

Local capacitance measurements from the SETSE provide topographical information complementary to electric field data. As an example, we mapped the surface potential (Fig. 5E) and local capacitance (Fig. 5F) extracted from the phase and period of $I_{SET}(V_b)$ acquired across the surface as described for Fig. 1. The two gate stripes seen traversing the image were held at the same potential as the 2DEG. In Fig. 5F, the increased proximity of the SET probe passing over the 30-nm-high gates causes a 20% rise in the capacitance signal; in contrast to other capacitance-based scanned probe techniques and because of the small well-defined island size, there is less stray capacitance background, enabling a more quantitative measurement. Furthermore, the SETSE can be operated at frequencies approaching dc, permitting the study of systems with slow response.

Further improvement of the SETSE will involve development of SETs and probes with higher sensitivity or smaller dimensions. The resolution of the present SETSE could be increased to perhaps 10 nm (*18*) with smaller fibers and tips and somewhat thinner films. This design would increase the operating temperature in proportion. Even room-temperature operation, although ambitious, is conceivable, requiring the development of molecular- or even atomic-sized SET tips.

There are a number of fundamental and applied problems that might benefit from this microscopic technique with its sensitivity to potential, charge, capacitance, contact potential, conductance, and dielectric composition. For instance, the properties of the electrons in the quantum Hall regime and their edge states (*19*) are attractive subjects for SETSE experiments. In principle, single-electron capacitance spectroscopy (*20*), which is a powerful technique for recording the complete electron energy structure of mesoscopic systems, could be implemented with the SETSE to add spatial mapping capability.

## REFERENCES AND NOTES


1. Y. Martin, Ed., *Scanned Probe Microscopies* (International Society of Optical Engineering, Washington, DC, 1995).
2. C. C. Williams, J. Slinkman, W. P. Hough, H. K. Wickramasinghe, *Appl. Phys. Lett.* **55**, 1662 (1989).
3. M. Nonnenmacher, M. P. Ogoyle, H. K. Wickramasinghe, *ibid.* **58**, 2921 (1991); A. K. Henning *et al.*, *J. Appl. Phys.* **77**, 1888 (1995).
4. Y. Martin, D. W. Abraham V. Raineri, H. K. Wickramasinghe, *Appl. Phys. Lett.* **52**, 1103 (1988).
5. C. Schoenenberger and S. F. Alvarado, *Phys. Rev. Lett.* **65**, 3162 (1990); C. Schoenenberger, *Phys. Rev. B* **45**, 3861 (1992).
6. T. A. Fulton and G. J. Dolan, *Phys. Rev. Lett.* **59**, 109 (1987); L. S. Kuzmin and K. K. Likharev, *JETP Lett.* **45**, 389 (1987); D. V. Averin and K. K. Likharev, in *Mesoscopic Phenomena in Solids*, B. L. Altshuler, P. A. Lee, R. A. Webb, Eds. (North-Holland, Amsterdam, 1991), pp. 173–271; see also H. Grabert and M. H. Devoret, Eds., *Single Charge Tunneling* (Plenum, New York, 1992).
7. The net charge on the island is an integral number of electrons. Any (nonintegral) variable charge induced on the island by external sources is compensated by charges of opposite sign induced by the capacitance to other electrodes, primarily that of the tunnel junctions to the source and drain. For the SETs used here, typical numbers are voltage biases ~1 mV, temperatures <2 K (required so that the thermal energy $kT < e^2/C$), currents ~1 nA with field-induced variations of ~50%, total island capacitances of ~0.1 fF, and sample-to-island capacitance of ~0.001 to 0.01 fF. Scanning electron micrographs show typical island diameters of 100 nm.
8. The field measurements referred to in the text are more accurately measurements of the electric flux terminating on the tip island. One must also allow for distortion of the field from the presence of the metal electrodes of the tip, particularly in proximity to a conductor, where the surface fields are altered to a greater degree.
9. Such substrates were fabricated from bare 80-μm-diameter single-mode optical fiber by a process described by E. Betzig, J. K. Trautman, T. D. Harris, J. S. Weiner, and R. L. Kostelak [*Science* **251**, 1468 (1991)].
10. The 2DEG has an areal density of $2 \times 10^{11}$ electrons per square centimeter.
11. Surface charges from sources other than the ionized silicon donors and their electrons pinned at the surface, such as surface debris or surface ions [K. Domansky, Y. Leng, C. C. Williams, J. Janata, D. Petelenz, *Appl. Phys. Lett.* **63**, 1513 (1993)], might also contribute. However, it is not necessary to invoke such additional sources to explain the data.
12. The sinusoidal dependence approximately describes the observed behavior at the comparatively high temperatures and magnetic fields that were used.
13. In this expression, $V_s$ is determined only modulo $e/C_s$, and the values are chosen so that $V_s$ varies smoothly with position within a map.
14. Because variations in the work function can be modeled as a charge dipole layer at the conducting surface, there is ambiguity in distinguishing between unresolved charge layers close to the electrode and variations in work functions.
15. The flux terminates on the tip and the 2DEG in rough proportion to their distances from a centered charge weighted by the dielectric constants with the 2DEG receiving most of the flux.
16. C. F. Eyring, S. S. McKeaown, R. A. Millikan, *Phys. Rev.* **31**, 900 (1928).
17. I. A. Larkin and V. B. Shikin, *Phys. Lett. A* **151**, 335 (1990).
18. SETs having sharpened tips showed good response at 4.2 K in preliminary tests and might display resolutions of order 50 nm.
19. D. B. Chlovskii, K. A. Matveev, B. I. Shklovskii, *Phys. Rev. B* **47**, 12605 (1993).
20. R. C. Ashoori, *Nature* **379**, 413 (1996).
21. The plot is actually of the induced charge divided by the fixed capacitance measured over the 2DEG. Off of the edge, the capacitance drops, but this variance was not incorporated here.


22. We thank G. Baraff, A. M. Chang, J. P. Eisenstein, B. I. Halperin, P. Mitra, and A. Yacoby for useful discussions.

17 December 1996; accepted 21 February 1997